



ENHANCEMENT OF THE TPD/AGO NPS HYBRIDE PHOTODETECTOR BY ADDING PEDOT PSS[†]

 **Shahlaa Majid J.***,  **Omar Adnan**

Department of Physics, College of Science, University of Baghdad, Baghdad, Iraq

**Corresponding Author e-mail: shahlaa.maged1204a@sc.uobaghdad.edu.iq*

Received January 13, 2023; revised February 1, 2023; accepted February 2, 2023

A photodetector was prepared by fusing AgO nanoparticles with a Alkyl-TPD (N'-diphenylbenzidine) polymer and depositing a TPD:AgO mixture on PS substrates using a spin coating technique. The response time of the synthesized (PSi/TPD:AgO) detector (by using a tungsten lamp with a 250 W/cm²) and its value (0.35 s) were measured in seconds. The detection, specificity, and photoresponse were (6.23×10⁸ W⁻¹, 3.611×10⁸ W⁻¹Hz^{1/2}cm, and 19.072×10⁻³ A/W). Hall measurements show that n-type nanoparticles have a carrier concentration of about (-1.15×10¹⁷ cm⁻³). With the addition of Poly(3,4-ethylenedioxythiophene):poly(styrene sulfonate) (PEDOT:PSS) polymer, the detection, specificity, optical response, and detector response time were improved to (80.06×10⁸ W⁻¹, 46.4×10⁸ W⁻¹Hz^{1/2} cm, 2019.48×10⁻³ A/W, and 5.3 ms), respectively.

Keywords: *Characteristics; Photocurrent Gain; Hall Effect; Specific Detectivity; Response Time*

PACS: 73.61.Ph, 78.20.-e, 78.66.-w, 78.66.Qn

1. INTRODUCTION

In the modern science landscape, AgO NPs are a well-known metal oxide whose popularity is on the rise due to its prevalence in a wide various possible application, Biomedical, zinc/silver oxide batteries, photovoltaic devices, optical switching, optical devices, magneto optical storage systems, sensors, the manufacture of nanoscale electronics, and oxidation analysis are all examples of applications for nanoscale electronics [1–4]. Silver being various forms and numerous phases the same as Ag₂O, Ag₃O₄, AgO, and Ag₂O₃, which are examples of inorganic materials, belong to this category [5–8]. Silver nanoparticles (AgNPs) have piqued the interest of many researchers and scientists due to their unique properties in physical, chemical, and biological fields when compared to their macroscale counterparts [2,13].

Experimentally, the researchers discovered that Ag₂O and AgO are more prevalent in visible phases than multivalent silver oxide (Ag₃O₄, Ag₂O₃) and have a high capacity specified [6, 7]. Several authors [9, 10] have investigated the fabrication and characteristics of silver and silver oxide thin films utilizing diverse approaches, radio frequency magnetron sputtering, the vapor solid liquid technique, etc. (The optical band gap of Ag₂O is highly dependent on its fabrication procedure). The use of nanoparticles of silver oxide containing a lattice parameter of 0.472 nm and a simple cubic structure as effective detergents catalysts for the activation of alkanes and olefin epoxidation, preservatives, colorants, and electrode materials is widespread in many industrial applications [11]. Due to its substantial optical band gap (2.5–3.1 eV), silver oxide is infrared transparent and can be seen. Silver nanoparticles (AgNPs) have piqued the interest of many researchers and scientists due to their unique properties in physical, chemical, and biological fields when compared to their macroscale counterparts [12,13]. Enabling the creation of a glass electrode and an antireflective coating for applications in the opto electrical field. In addition, silver oxide can be used to store data in both optical and magneto-optical ways. Silver oxide can reflect more than 70% of light over a wide range of wavelengths. This is useful because the material can be used to store short-wavelength optical data; an inorganic storage substance is used instead of the organic storage substance that was used before. Tominaga et al. [14]. In contrast to copper, which can be quickly oxidized at high temperatures and from which single crystals of Cu₂O may be produced, the brittleness of the silver-oxygen link limits the use of this method to produce Ag₂O unless extremely high oxygen pressures are used [15]. Once formed, Ag₂O is stable at ambient temperature but begins to disintegrate at over 60°C in a vacuum. In an HF-rich electrolyte; silicon is etched electrochemically to produce porous silicon (PS). Its structure is complicated, with nanometer-sized pores dispersed throughout a random network. The interesting features of the nanostructured silicon that constitutes the material's backbone result primarily from the electron-hole couples are quantum-confined. In recent years, visible light emission in response to optical and electrical pumping at room temperature has been recorded [16, 17]. PS has been shown to be useful in other ways as a passive material [18, 19, 20, 21]. For example, changing the electrochemical current over time while the material is growing makes it easy to make structures with multiple layers that can function as distributed Bragg reflectors (DBRs) [22, 23], microcavities [24], waveguides [25], etc. Alkyl-TPD (N'-diphenylbenzidine) is a typical substance with a 5.5 eV ionization potential and excellent transport hole mobility of 10³ cm²/Vs [26, 27]. TPD is often used in phosphorescence-organic light-emitting diodes as a blue-violet light-emitting material or host material due to its approximately 3.2 eV energy band wide, having the most molecular orbitals occupied (HOMO) and the lowest unoccupied molecular orbital (LUMO) of -5.5eV and -2.3 eV, respectively [28].

One of the most promising conductive polymers is poly(3,4-ethylenedioxythiophene):poly(styrene sulfonate) (PEDOT:PSS) [29-31]. During the last two decades, research on PEDOT:PSS has increased dramatically [32]. Polymer

[†] Cite as: M.J. Shahlaa, and O. Adnan, East Eur. J. Phys. 1, 246 (2023), <https://doi.org/10.26565/2312-4334-2023-1-33>

© M.J. Shahlaa, O. Adnan, 2023

photodetectors have drawn tremendous attention due to their inherent advantages of solution-based and low-cost fabrication, mechanical flexibility, and light weight over their inorganic counterparts [33–36]. In this study, more than one detector was manufactured to study the effect of adding PEDOTPSS. PSI (Poros silicon) was used as the substrate in all photodetectors manufactured.

2. EXPERIMENTAL WORK

Silver oxide was prepared by pulsed laser ablation method. The Nd:YAG laser utilized in the deformation process operates at a frequency of 6 Hz with a pulse width of 7 ns and a wavelength of 1064 nm. The laser pulses were concentrated on a 20 cm positive lens on a 2 mm dry AgO bulk specimen that had been moistened in chloroform with a laser power of 1000 mJ and 2000 shots. As a substrate, a monocrystalline a wafer of n-type silicon with an electrical resistivity of (0.008-0.02) $\Omega \cdot \text{cm}$ and (111) orientation was utilized. In order to get rid of the native oxygen, the wafer was immersed in 40% HF. Electrochemical etching (anodization) in a solution of ethanoic hydrofluoric acid at a current density of 20 mA/cm² for 20 minutes in the dark at 300K was used to make the porous layer. So that an oxide layer wouldn't form on top of the porous silicon film, ethanol was often added. The samples were then cleaned and air dried. A [TPD Polymer -chloroform] solution was prepared by dissolving 0.075 g of TPD in 3 ml of chloroform and stirring the mixture until completely dissolved.

- The fabrication of photodetector device is manufactured as follows:
 - p-TPD is used to form the photodetector's active layer by mixing a solution of AgO nanoparticles and p-TPD-chloroform in a mole ratio of 2:1.
 - The detector was then created by spin coating a TPD:AgO mixture on PSi. The mixture of AgO:TPD is deposited on PSi at 3000rpm for 15 seconds. After PSi/AgO:TPD has been precipitated. After that, it is put in an oven at a temperature of 50 degrees Celsius for 30 minutes.
- The fabrication of improved detector was started by add deposition of PEDOTPSS on PSi substrate .Then, it is deposited at a speed of 1,500 revolutions per minute for a duration of 30 seconds. After the precipitation process is done, the PSi/PEDOTPSS is put in an oven at 120°C for 20 minutes to matching with the substrate .The mixture of AgO:TPD is deposited on PSi/PEDOTPSS at 3000rpm for 15 seconds. After PSi/PEDOTPSS/AgO:TPD has been precipitated. After that, it is put in an oven at a temperature of 50 degrees Celsius for 30 minutes.

3. RESULTS AND DISCUSSION

3.1. MORPHOLOGICAL PROPERTIES

SEM images display clusters of spherical, bright spots (circles and inset picture) that correspond to silver oxide nanoparticles, with an average particle size of about (22-26) nm as shown in Fig.1.

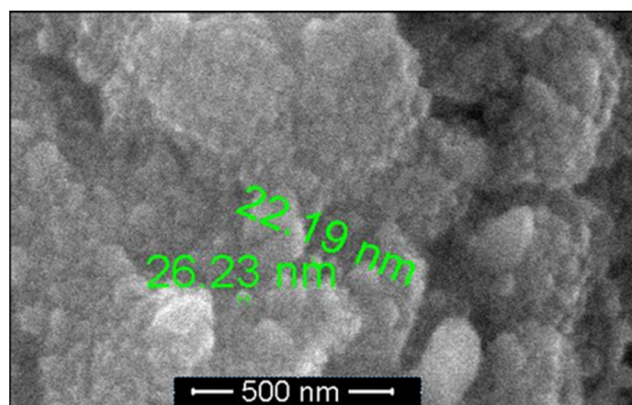


Figure 1. SEM image of AgO NPs.

3.2. OPTICAL PROPERTIES OF AGO NANOPARTICLES

UV–Vis spectroscopy, photoluminescence (PL) spectra, and FTIR spectroscopy were utilized to determine the optical characteristics of the AgO nanostructure. As seen in Fig. 2, the absorption spectra have a peak at 300 nm. Quantum-size impact is indicated by a blue shift in the absorption spectrum compared to the peak absorbance of AgO in bulk. Using the Tauc relation, calculate the optical bandgap energy (E_g) of the semiconductor [37]. A plot of $(h\nu)^2$ versus $h\nu$ shows a linear region of intermediate extrapolation of the linear portion can be used to determine E_g from the intersection with the $(h\nu)$ axis, as depicted in Fig.3. The calculated values of E_g for AgO are about 3.06 eV. PL spectra spectrum was shown in Fig.5. A 300 nm source is used to excite the specimen. Fitting Gaussian-shaped peaks to the PL spectrum and are centered at about 402 nm. The PL spectra of the NPs implies that there exist more defect energy levels (trap states or surface states) at 467 nm and 601 nm.

The FTIR spectra of AgO NPs were recorded at 3429.2 cm^{-1} for the alcohol stretching vibration (OH group), 2925.8 cm^{-1} for the vibrational stretching of the C-H methyl and methylene bonds, 1639.38 cm^{-1} for the stretching

vibration of the C=O bonds in pectin ester and carboxylic acid, etc. [38]. The weak band at 588.25 cm^{-1} attributable to the Ag-O vibration consists of those for crystal (lattice) and coordinated water in addition to Ag_2O . The obtained characteristic absorption band at 889.12 cm^{-1} is explained by the stretching and bending vibrations of Ag-O [39].

3.3. ELECTRICAL CHARACTERISTICS OF NANOPARTICLES AGO

1) Hall Effect

To analyze the electrical properties of AgO, the Hall Effect setup type (HMS3000) is utilized. The 600-nanometer-thick sheet exhibits n-type conductivity, characteristic of semiconductors. The mobility was $1.13 \times 10^3 (\text{cm}^2/\text{V}\cdot\text{sec})$, the conductivity and resistivity were $2.07 \times 10^1 (\Omega \cdot \text{cm})^{-1}$ and $4.83 \times 10^{-2} (\Omega \cdot \text{cm})$. The carrier concentration is $-1.15 \times 10^{17}\text{ cm}^{-3}$. The Hall coefficient $-5.45 \times 10^1 (1/\text{Cm}^3 \cdot \text{C})$.

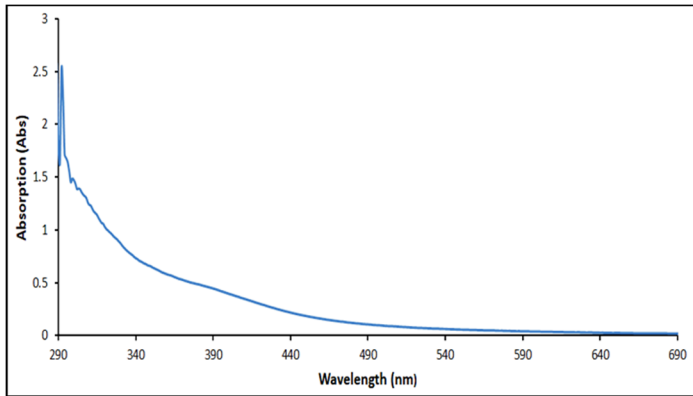


Figure 2. The absorption spectrum AgO nanoparticles

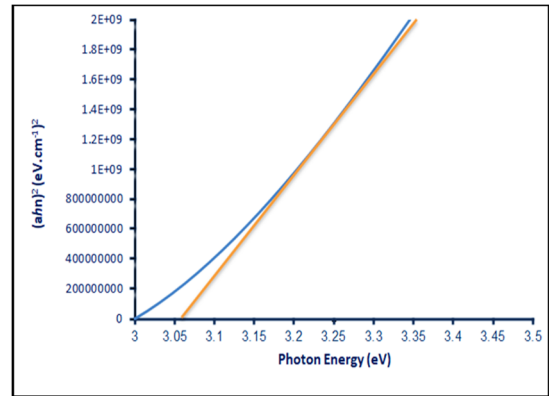


Figure 3. $(\alpha h\nu)^2$ vs. photon energy for AgO nanoparticles

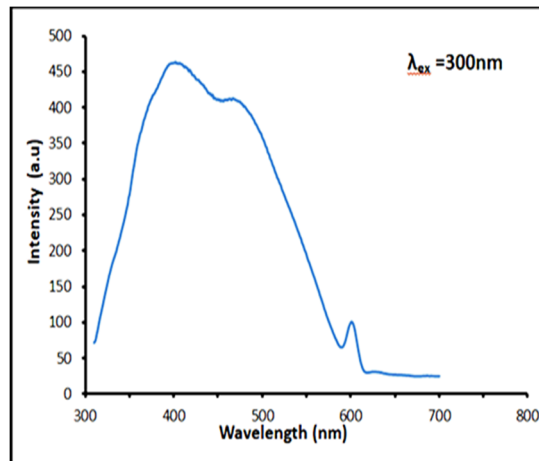


Figure 4. Photoluminescence spectrum of AgO nanoparticle.

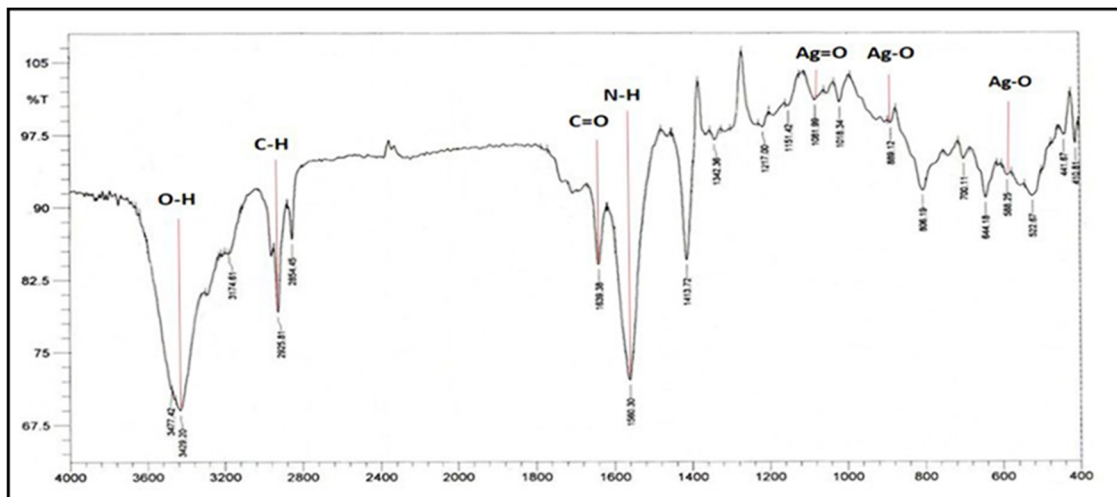


Figure 5. FTIR spectra for pure AgO NPs thin film.

2) Current–voltage measurements

The current-voltage (I–V) properties of the photodetector are examined as a function of the bias voltage in the absence and presence of a 250-W tungsten halogen lamp. At room temperature, a rise in current was noticed. Figure 6 displays I–V characteristics of PSi/TPD:AgO photodetector and PSi/PEDOTPSS/TPD:AgO photodetector. Curves of current–voltage are the most often employed device characterization technique. The current densities of the detectors were 4.768 A/cm² and 504.87 A/cm², respectively.

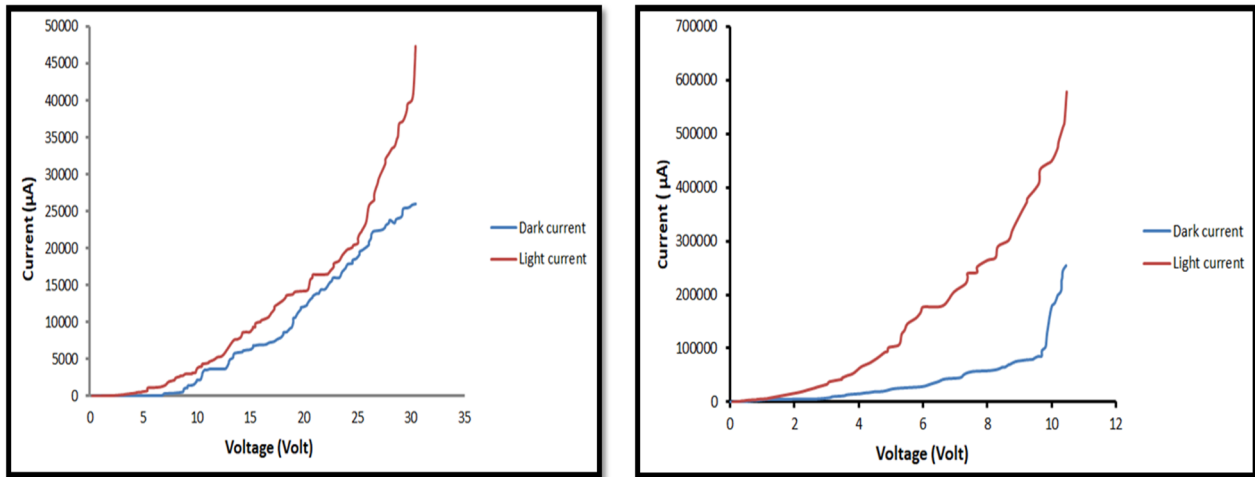


Figure 6. I–V characteristics of (a) PSi/TPD:AgO photodetector (b) PSi/PEDOTPSS/TPD:AgO photodetector

Calculated by dividing the photocurrent by the dark current at the same bias voltage, the photoconductive gain (G) is given by $G = \tau/T$, where T is the transient time between the detector electrodes and $\tau =$ is the charge carrier life time. The photocurrent gain of the PSi/ TPD:AgO detector was 1.447 while that of the PSi/TPD:AgO detector was 2.25. Using the value of gain G and the transit time for detectors The carries life time was found to be about 1.447 sec, 0.045 sec for PSi/TPD:AgO detector and PSi/PEDOTPSS/TPD:AgO detector respectively. There is a correlation between electrode separation and carrier mobility, which in turn has an effect on the transient time; $T=L^2/\mu V$, where L is the distance between the electrodes, μ is the carrier mobility, and V is the bias voltage. Using the value of transient time, electrode spacing and the bias voltage. The mobility of the carrier was found to be about 145.4×10^{-6} (cm²/V·sec) and 7272.7×10^{-6} (cm²/V·sec) for each detector respectively.

The prepared samples' Johnson noise is calculated using the equation:

$$I_n = (4K_B T \Delta f / R)^{1/2}, \tag{1}$$

where K_B is Boltzmann constant, R is resistance of photodetector, and T is temperature.

The Johnson noise of the PSi/TPD:AgO detector was 2.6808×10^{-9} A while that of the PSi/PEDOTPSS/TPD:AgO detector was 27.075×10^{-9} A.

Responsivity of the prepared samples is determined using equation:

$$R_\lambda = J / P_{opt}, \tag{2}$$

where J is the current density of the photodetector in (A/cm²), P_{opt} is the incident radiation power and its value (250 Watt/cm²).

The greatest values of the responsivity calculated by the PSi/PEDOTPSS/AgO:TPD photodetector. PSi/ TPD:AgO responsivity was 19.072×10^{-3} A/Watt, and PSi/TPD: AgO responsivity was 2019.48×10^{-3} A/Watt.

The specific detectivity D^* , referred to also as the normalized detectivity, which is the inverse of normalized noise equivalent power (NEP). To the detector area of 0.336 cm² and a noise electrical band width of 1 Hz. This reciprocal can be expressed as follows:

$$D^* = R_\lambda (A \Delta f)^{1/2} / I_n \tag{3}$$

Where R_λ is the optical response of the photodetector in (A/Watt), A is the sensitive area of the detector and I_n is the noise current is calculated from the dark current using the following formula:

$$I_n = (2 e I_d \Delta f)^{1/2}. \tag{4}$$

Where I_d represents the dark current, e represents the electron charge, and Δf represents the noise bandwidth, which results in a noise current for the PSi/TPD: AgO detector of about (3.057×10^{-11} A) and for the PSi/PEDOTPSS/AgO:TPD detector of about (25.226×10^{-11} A), at $\Delta f = 1$ Hz.

Utilizing the photosensitivity value, $A = 0.336 \text{ cm}^2$, the specific detectivity of PSi/TPD:AgO detector ($3.611 \times 10^8 \text{ Watt}^{-1} \text{ Hz}^{1/2} \text{ cm}$) and of PSi/PEDOTPSS/AgO:TPD detector ($46.4 \times 10^8 \text{ Watt}^{-1} \text{ Hz}^{1/2} \text{ cm}$).

The quantum efficiency is associated with the responsivity of the detector and calculated using the equation:

$$\eta = \frac{1240}{\lambda} R_{\lambda} \quad (5)$$

The quantum efficiency of PSi/TPD:AgO detector (36.383×10^{-3}), and of PSi/PEDOTPSS/TPD:AgO detector (3852.5×10^{-3}).

The addition of PEDOTPSS material increased the response time and the quantum efficiency. This means that this addition is useful for device optimization.

4. CONCLUSION

The PSi/TPD:AgO detector was prepared using silicon electrochemical etching, mixing silver oxide with TPD polymer, and depositing the TPD:AgO mixture by spin-coating method. PEDOTPSS was then deposited by spin-coating to prepare the PSi/PEDOTPSS/TPD:AgO detector. The addition of PEDOTPSS significantly improved the optical conductivity gain from 1.447 to 2.25. The luminous response has been increased from $19.072 \times 10^{-3} \text{ (A/Watt)}$ to $2019.48 \times 10^{-3} \text{ (A/Watt)}$, as has the response time range from 0.35 seconds to 0.0053 seconds.

ORCID IDs

Shahlaa Majid J., <https://orcid.org/0000-0002-0595-6293>; Omar Adnan, <https://orcid.org/0000-0003-3709-5245>

REFERENCE

- [1] S. Ravichandran, V. Paluria, G. Kumar, K. Loganathan, and B.R.K. Venkata, "A novel approach for the biosynthesis of silver oxide nanoparticles using aqueous leaf extract of *Callistemon lanceolatus* (Myrtaceae) and their therapeutic potential", *J. Exp. Nanosci.* **11**, 445458 (2016). <https://doi.org/10.1080/17458080.2015.1077534>
- [2] M. Limbitot, S. Kalyane, N. Sharanappa, S. Manjula, and B. Evale, "Electrical and dielectric studies of silver oxide doped polyaniline [AgO/PANI] nanocomposite", *Int. J. Adv. Sci. Res.* **3**, 87–93 (2018).
- [3] Z.H. Dhoondia, and H. Chakraborty, "Lactobacillus mediated synthesis of silver oxide nanoparticles", *Nanopart. Nanomater. Nanotechnol.* **2**, 1–7 (2012). <https://doi.org/10.5772/55741>
- [4] S. Sagadevan, "Synthesis, Structural, surface morphology, optical and electrical properties of silver oxide nanoparticles", *Int. J. Nanoelectron. Mater.* **9**, 37 (2016).
- [5] M.A. Hassan, I.R. Agool, and L.M. Raoof, "Silver Oxide Nanostructured Prepared on Porous Silicon for Optoelectronic Application", *Appl. Nanosci.* **4**(4), 429 (2014). <https://doi.org/10.1007/s13204-013-0215-z>
- [6] G. Saroja, V. Vasu, and N. Nagarani, "Optical Studies of Ag₂O Thin Film Prepared by Electron Beam Evaporation Method", *O J. Metal.* **3**, 57 (2013). <http://dx.doi.org/10.4236/ojmetal.2013.34009>
- [7] P. Kavitha, S. Suseela, and M. Mary, "Synthesis and Characterization of Cadmium Sulfide Nanoparticles", *Int. J. Eng. Sci.* **2**(3), 108-110 (2013). <https://theijes.com/papers/v2-i3/Q02301080110.pdf>
- [8] B. Reidy, A. Haase, A. Luch, K.A. Dawson, and I. Lynch, "Mechanisms of Silver Nanoparticle Release, Transformation and Toxicity: A Critical Review of Current Knowledge and Recommendations for Future Studies and Applications", *Materials*, **6**(6), 2295 (2013). <https://doi.org/10.3390/ma6062295>
- [9] F.X. Bock, T.M. Christensen, S.B. Rivers, L.D. Doucette, R.J. Lad, "Growth and Structure of Silver and Silver Oxide Thin Films On Sapphire", *Thin Solid Films*, **468**(2-1), 57–64 (2004). <https://doi.org/10.1016/j.tsf.2004.04.009>
- [10] Q. Tian, D. Shi, and Y. Sha, "CuO and Ag₂O/CuO Catalyzed Oxidation of Aldehydes to The Corresponding Carboxylic Acids by Molecular Oxygen", *Molecules*, **13**(4), 948-957 (2008). <https://doi.org/10.3390/molecules13040948>
- [11] S. Wang, H. Li, H. Yu, J. Yu, and S. Liu, "Ag₂O as a new visible light photocatalyst: self-stability and high photocatalytic activity," *Chemistry A European Journal*, **17**(28), 7777 (2011). <https://doi.org/10.1002/chem.201101032>
- [12] S. Agrawal, M. Bhatt, S. Rai, A. Bhatt, P. Dangwal, and P. Agrawal, "Silver nanoparticles and its potential applications: a review", *J. Pharmacogn. Phytochem.* **7**, 930e937 (2018). <https://www.phytojournal.com/archives?year=2018&vol=7&issue=2&ArticleId=3470>.
- [13] M. Alhamid, B. Hadi, and A. Khumaeni, "Synthesis of silver nanoparticles using laser ablation method utilizing Nd:YAG laser", *AIP Conf. Proc.* **2202**, 020013 (2019). <https://doi.org/10.1063/1.5141626>
- [14] J. Tominaga, T. Nakano, and N. Atoda, *Extended Abstracts of the 39th Spring Meeting of the Japan Society of Applied Physics and Related Societies*, (Nippon Univ. Narashino, 30 aL-3, 1993).
- [15] Von E. Menzel, and C. Menzel-Kopp, *Z. Naturf.* **13a**, 986 (1958). https://zfnpmpdl.mpg.de/data/Reihe_A/13/ZNA-1958-13a-0985.pdf
- [16] L.T. Canham, *Appl. Phys. Lett.* **57** (10), 1046 (1990). <https://doi.org/10.1063/1.103561>
- [17] A. Halimaoui, C. Oules, G. Bomchil, A. Bsiesy, F. Gaspard, R. Herino, M. Ligeon and F. Muller, *Appl. Phys. Lett.* **59** 304 (1991). <https://doi.org/10.1063/1.105578>
- [18] M.J. Sailor, in *Properties of Porous Silicon*, edited by L.T. Canham, (IEE Inspec., London, 1997), pp. 364.
- [19] W. TheiB, *Surf. Sci. Rep.* **29**(3/4), 91 (1997). [https://doi.org/10.1016/S0167-5729\(96\)00012-X](https://doi.org/10.1016/S0167-5729(96)00012-X)
- [20] M.V. Wolkin, S. Chan, and P.M. Fauchet, *Phys. Stat. Sol. (a)*, **182**, 573 (2000). [https://doi.org/10.1002/1521-396X\(200011\)182:1%3C573::AID-PSSA573%3E3.0.CO;2-G](https://doi.org/10.1002/1521-396X(200011)182:1%3C573::AID-PSSA573%3E3.0.CO;2-G)
- [21] W. Liu, et al., *J. Vac. Sci. & Techn. B*, **21**, 168 (2003). <https://doi.org/10.1116/1.1537714>
- [22] M.G. Berger, R. Arens-Fischer, M. Kruger, S. Billat, H. Luth, S. Hilbrich, W. TheiB, and P. Grosse, *Thin Solid Films*, **297**, 237 (1997). [https://doi.org/10.1016/S0040-6090\(96\)09361-3](https://doi.org/10.1016/S0040-6090(96)09361-3)
- [23] V. Agarwal, and J.A. del Rio, *Appl. Phys. Lett.* **82**, 1512 (2003). <https://doi.org/10.1063/1.1559420>
- [24] L. Pavesi, *Riv. Nuovo Cim.* **20**, 1 (1997). <https://doi.org/10.1007/BF02877374>

- [25] S. Nagata, C. Domoto, T. Nishimura, and K. Iwameji, *Appl. Phys. Lett.* **72**, 2945 (1998). <https://doi.org/10.1063/1.121502>
- [26] J.A. Chilton, and M.T. Goosey, editors, *Special polymer for electronics and optoelectronics*, (Chapman and Hall, London, 1995), pp. 351, ISBN 0-412-58400-X
- [27] Csavinszky, P. (1978). Quantum Mechanical Treatment of Transport Properties of Semiconductors: Possible Application to Polymers, in: *Quantum Theory of Polymers, NATO Advanced Study Institutes Series*, edited by J.M. André, J. Delhalle, and J. Ladik, vol 39, (Springer, Dordrecht, 1978). https://doi.org/10.1007/978-94-009-9812-4_15
- [28] F. Wang, Z. Chen, L. Xiao, B. Qu, and Q. Gong, “Enhancement of the power conversion efficiency by expanding the absorption spectrum with fluorescence layer”, *Optics Express*, **19**, A361–A368 (2011). <https://doi.org/10.1364/OE.19.00A361>
- [29] X. Yang, and M. Zhang, “Review of flexible microelectromechanical system sensors and devices”, *Nanotechnol. Precis. Eng.* **4**(2), 025001 (2021). <https://doi.org/10.1063/10.0004301>
- [30] Y. Chang, J. Zuo, H. Zhang, et al., « State-of-the-art and recent developments in micro/nanoscale pressure sensors for smart wearable devices and health monitoring systems”, *Nanotechnol. Precis. Eng.* **3**(1), 43 (2020). <https://doi.org/10.1016/j.npe.2019.12.006>
- [31] M. Sun, and X. Duan, “Recent advances in micro/nanoscale intracellular delivery”, *Nanotechnol. Precis. Eng.* **3**(1), 18 (2020). <https://doi.org/10.1016/j.npe.2019.12.003>
- [32] H. Shi, C. Liu, Q. Jiang, and J. Xu, “Effective approaches to improve the electrical conductivity of PEDOT:PSS review”, *Adv. Electron. Mater.* **1**(4), 1500017 (2015). <https://doi.org/10.1002/aelm.201500017>
- [33] C. Fuentes-Hernandez, W.-F. Chou, T.M. Khan, L. Diniz, J. Lukens, F.A. Larrain, V.A. Rodriguez-Toro, and B. Kippelen, *Science*, **370**, 698-701 (2020). <https://doi.org/10.1126/science.aba2624>
- [34] C. Li, H. Wang, F. Wang, T. Li, M. Xu, H. Wang, Z. Wang, et al., *Light Sci. Appl.* **9**, 31 (2020). <https://doi.org/10.1038/s41377-020-0264-5>
- [35] X. Ma, A. Zeng, J. Gao, Z. Hu, C. Xu, J.H. Son, S.Y. Jeong, et al., *Natl. Sci. Rev.* **8**, nwa305 (2021). <https://doi.org/10.1093/nsr/nwaa305>
- [36] Z. Hu, Z. Wang, Q. An, and F. Zhang, *Sci. Bull.* **65**, 131 (2020). <https://doi.org/10.1016/j.scib.2019.09.016>
- [37] J.I. Pankov, *Optical Processes in Semiconductors*, (Prentice-Hall, Englewood Cliffs, 1971).
- [38] V. Manikandan, P. Velmurugan, J.-H. Park, W.-S. Chang, Y.-J. Park, P. Jayanthi, M. Cho, and B.-T. Oh, “Green synthesis of silver oxide nanoparticles and its antibacterial activity against dental pathogens,” *3 Biotech*, **7**(1), 72 (2017). <https://doi.org/10.1007/s13205-017-0670-4>
- [39] A. Rita, A. Sivakumar, S.S.J. Dhas, and S.A. Martin Britto Dhas, “Structural, optical and magnetic properties of silver oxide (AgO) nanoparticles at shocked conditions”, *J. Nanostruct. Chem.* **10**, 309 (2020). <https://doi.org/10.1007/s40097-020-00351-z>

ПОКРАЩЕННЯ ГІБРИДНОГО ФОТОДЕТЕКТОРА TPD/AGO NPS ШЛЯХОМ ДОДАВАННЯ PEDOT PSS

Шахла Маджид Дж., Омар Аднан

Факультет фізики, Науковий коледж, Багдадський університет, Багдад, Ірак

Фотодетектор був виготовлений шляхом сплавлення наночастинок AgO з полімером алкіл-TPD (N'-дифенілбензидину) та нанесення суміші TPD:AgO на підкладки з полістиролу за допомогою технології спінування. Час відгуку синтезованого (PSi/TPD:AgO) детектора (за допомогою вольфрамової лампи з потужністю 250 Вт/см²) та його значення (0,35 с) вимірювали в секундах. Виявлення, специфічність і фотовідгук становили (6,23×10⁸ Вт, 1, 3,611×10⁸ Вт⁻¹Гц^{1/2}·см і 19,072×10⁻³ А/Вт). Вимірювання Холла показують, що наночастинки n-типу мають концентрацію носія приблизно (1,15×10¹⁷ см⁻³). З додаванням полімеру полі(3,4-етилендіокситіофен):полі(стиролсульфонат) (PEDOT:PSS) виявлення, специфічність, оптична відповідь і час реакції детектора були покращені до (80,06×10⁸ Вт⁻¹, 46,4×10⁸ Вт⁻¹Гц^{1/2}·см, 2019,48×10⁻³ А/Вт і 5,3 мс) відповідно.

Ключові слова: характеристики; посилення фотоструму; ефект Холла; питома чутливість; час відгуку